

Bound states in nonuniform superconductorsXiong Fan^{1,*} and Xi Dai^{1,2}¹*Department of Physics, Hong Kong University of Science and Technology, Hong Kong 999077, China*²*Materials Department, University of California, Santa Barbara, Santa Barbara, California 93106, USA* (Received 12 November 2022; revised 7 February 2023; accepted 21 March 2023; published 7 April 2023)

This paper shows that the WKB quantization rule is suitable for the Andreev bound states in nonuniform superconductors. We consider nonhomogeneous superconductivity gap functions $\Delta(x)$ in superconductors with the Bogoliubov quasiparticle energy E , the Fermi level E_F , and the total momentum \mathbf{p} at $E_F + E$. The Andreev bound states in the well of slowly varying $|\Delta(x)|$ are studied, and the well may also be induced by the phase variation of $\Delta(x)$ for massless Dirac fermions. By applying the WKB method to the Bogoliubov–de Gennes equation, we obtain two main results: (i) For $E_F \sim 0$, the bound states are determined by $\int_{L_E}^{R_E} |\mathbf{p} dx| = (\frac{1}{2} + n)\pi\hbar$, where $n \in \mathbb{N}_0$ and L_E and R_E are the boundary points between the classically allowed region and forbidden regions, and (ii) for $E_F \gg E$ and $|\Delta(x)|$, the bound states are given by $\int_{L_E}^{R_E} |\mathbf{p} \pm \mathbf{p}_F| dx = (\frac{1}{2} + n)\pi\hbar$ with small $p_{y(z)}$. Empirical quantization conditions are provided for broader parameter regions. In addition to applying the traditional WKB method, we also develop a generalized WKB method to tackle semimetals with parabolic dispersion relationships. The applications of our results are discussed, for example, Dirac π junctions or nonchiral Majorana wires, SNS junctions, the excitation threshold, and the tunneling rate in NSN junctions. In the π junction, the Majorana zero modes correspond to the zero-point energy in the WKB formalism. This observation may provide insights into the Majorana bound state in a vortex and the Majorana fermions in high-energy physics.

DOI: [10.1103/PhysRevB.107.134506](https://doi.org/10.1103/PhysRevB.107.134506)**I. INTRODUCTION**

The WKB method is a powerful tool in quantum mechanics [1,2]. For slowly varying potentials, the WKB method conveniently gives the approximate wave function, bound-state energy, and tunneling rate for the Schrödinger equation. In particular, this method gives the exact bound-state energy of the quantum harmonic oscillator after adding a correction $\frac{1}{2}\hbar$ to the Bohr-Sommerfeld quantization rule $\oint p dq = nh$. The pioneering researchers of this method, Wenzel [3], Kramers [4], Brillouin [5], and Jeffreys [6], discovered an effective treatment of the turning points between the classically allowed region and forbidden regions, which will be adopted in this paper. Compared with the WKB approximation, Ref. [7] gives an exact formula, which takes an additional integral form, to calculate the bound-state energy. In recent decades, the WKB method has been extended to several fields, for example, the supersymmetry WKB [8–11] advances in providing exact eigenvalues for shape-invariant potentials, although the ground-state wave function is a prerequisite; remarkably, the WKB approximation has been applied to the famous Wheeler-DeWitt equation in quantum gravity [12,13]; Caroli *et al.* [14] and Bardeen *et al.* [15] developed a method with the WKB approximation to solve the excitations in the vortex line in type-II superconductors and Beenakker and van Houten applied this method to bound states in superconducting constriction [16]. We note that in these applications of the WKB

approximation, problems are all about second-order differential equations. At the same time, Ref. [17] pointed out that the WKB method is also suitable for higher-order differential equations. In this paper, except for applying the traditional WKB method to massless Dirac fermions and Schrödinger fermions, we also provide an example, the Bogoliubov–de Gennes (BdG) equation of the semimetals with parabolic dispersion relationships, which is reduced to a fourth-order differential equation under specific conditions.

The present paper will discuss the bound states in the BdG equation with slowly varying gap functions. These bound states are important for thermodynamics and Josephson current in superconductors [16,18,19]. The study of the bound states in SNS junctions starts from Andreev’s levels. Andreev considered a square well of the gap function $\Delta(x)$, with $\Delta(x) = 0$ inside the normal layer, and obtained a series of discrete energy levels which are irrelevant to the phase difference of the superconductors on two sides. The physics of Andreev’s levels is elegant: An electron motion process and a hole motion process form a reflection period together in the reciprocating process. This behavior yields a standing wave in the normal layer [20,21]. Based on Andreev’s levels, Kulik made progress in connecting the phase difference between the two superconductors with the bound states by considering the phase coherence [22]. The gap functions considered in this paper are more general, for instance, the well in Fig. 1, where the electronlike and holelike excitations convert into each other at the boundary regions. In addition, the conversion may manifest through the retroreflection or specular reflection [23]. We assume that $\Delta(x)$ changes smoothly and slowly so

*xfanam@ust.hk

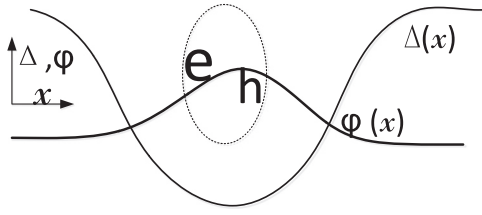


FIG. 1. Depiction of an Andreev bound state $\varphi(x)$, a mixed state of the electron and hole, in a well of $\Delta(x)$; $\varphi(x)$ roughly demonstrates the distribution probability of the bound state.

that the WKB method is suitable for applications. Our basic procedures conform to the insights of Wentzel *et al.* and Weinberg, and auxiliary techniques are developed to cope with the fourth-order differential equations, i.e., the generalized WKB (GWKB) method.

In the following sections we first prove the quantization conditions for the bound states given in the abstract. We study the massless Dirac fermions on the surface of a strong topological insulator (TI) in Sec. II, the semimetals with parabolic dispersion relationships in Sec. III, and Schrödinger fermions in normal metals in Sec. IV. Different parameter limits are targeted separately. The pairing potentials in the BdG equations may be inherent or induced by the proximity effect, and only the *s*-wave pairing is considered. After the proof of the quantization rules, we elaborate on some application examples in Sec. V [the $\pi(0)$ junction in Sec. II D]. We then discuss the significance and experimental realization of these bound states and generalize the quantization condition to broader parameter regions in Sec. VI. We summarize in Sec. VII. In addition, numerical simulations are provided in the Supplemental Material [24]. To simplify notation and without loss of clarity, we ignore spins in most of the discussion.

II. MASSLESS DIRAC FERMIONS

We consider the surface states of a strong TI with the Hamiltonian $H_0 = v_F(\hat{p}_x\sigma_x + \hat{p}_y\sigma_y) - E_F$, with v_F the Fermi velocity, $\hat{p}_{x(y)}$ the momentum operators in the *x* (*y*) direction, $\sigma_{x(y)}$ the Pauli matrices, and E_F the Fermi level. When an *s*-wave superconductor covers the surface states, the excitations are described by the Dirac–Bogoliubov–de Gennes (DBdG) equation [23,25]

$$\begin{pmatrix} H_0 & \Delta(x) \\ \Delta^*(x) & -H_0 \end{pmatrix} \begin{pmatrix} \Psi \\ \Phi \end{pmatrix} = E \begin{pmatrix} \Psi \\ \Phi \end{pmatrix}, \quad (1)$$

where the gap function or pairing function $\Delta(x) = \Delta_r e^{i\theta}$, with Δ_r a real function and θ the accompanying phase, and $\Delta(x)$ couples the electron spinor $\Psi = (\Psi_1, \Psi_2)^T$ and the hole spinor $\Phi = (\Phi_1, \Phi_2)^T$. Here $\Psi_{1(2)}$ denotes the up- (down-) spin electron component and $\Phi_{1(2)}$ denotes the down- (up-) spin hole component. The normalization condition is $\int (\Psi^\dagger \Psi + \Phi^\dagger \Phi) d\mathbf{r} = 1$. Similar equations can also be found in graphene sheets covered by superconducting layers. The excitation spectrum for uniform $\Delta(x)$ is $E = \sqrt{|\Delta|^2 + (E_F \pm \hbar v_F |\mathbf{k}|)^2}$, where the electronlike and holelike bands coincide when $E_F = 0$. Since we discuss the bound states in the one-dimensional well of the gap function, the translational invariance of the gap function breaks in the *x*

direction, while $\Delta(x)$ is translationally invariant in the *y* direction. Therefore, p_y is always a good quantum number. In the following, we discuss three limits of the parameters k_y and E_F : (i) $k_y \neq 0$ and $E_F \sim 0$, (ii) $k_y = 0$ and $E_F \neq 0$, and (iii) $|\hbar v_F k_y| \ll E_F$. In these situations, the BdG equation will be mapped to the Schrödinger equation. Except for these limits, our experience is that the obtained quantization condition of the Andreev bound states appertains to broader parameter ranges only if we find effective potentials and semiclassical momenta. As an application, the π junction and 0 junction are discussed in Sec. II D and the results are close to those obtained by the transfer-matrix method [18] despite different boundary conditions.

A. Case of $k_y \neq 0$ and $E_F \sim 0$

In this case, k_y is a good quantum number. Therefore, we assume $\Psi(y)$ and $\Phi(y) \propto e^{ik_y y}$, and p_y can be regarded as a fixed parameter. The substitutions of the second and third equations into the first and fourth equations in the system of equations yield

$$\begin{aligned} v_F^2 \hat{p}_x^2 \Psi_1 - i\hbar v_F (\partial_x \Delta) \Phi_2 &= (E^2 - \Delta \Delta^* - v_F^2 p_y^2) \Psi_1, \\ v_F^2 \hat{p}_x^2 \Phi_2 + i\hbar v_F (\partial_x \Delta^*) \Psi_1 &= (E^2 - \Delta \Delta^* - v_F^2 p_y^2) \Phi_2. \end{aligned} \quad (2)$$

If the $\partial_x \Delta$ and $\partial_x \Delta^*$ terms are negligible, we have the relationship $\int_{L_E}^{R_E} p_x dx = (\frac{1}{2} + n)\pi\hbar$ by letting $p_x = (E^2 - \Delta \Delta^* - v_F^2 p_y^2)^{1/2}/v_F$. Recall that L_E and R_E denote the left and right boundary points between the classically allowed and forbidden regions. We can also include the $\partial_x \Delta$ and $\partial_x \Delta^*$ terms. Using the substitution

$$\Psi_1 = \pm \frac{\Delta(x) \partial_x \theta(x) - i e^{i\theta(x)} \partial_x \Delta_r(x)}{\sqrt{\Delta_r^2(x) [\partial_x \theta(x)]^2 + [\partial_x \Delta_r(x)]^2}} \Phi_2, \quad (3)$$

we obtain

$$\begin{aligned} v_F^2 \hat{p}_x^2 \Psi_1 &= (E^2 - \Delta \Delta^* - v_F^2 p_y^2 \mp V_0) \Psi_1, \\ v_F^2 \hat{p}_x^2 \Phi_2 &= (E^2 - \Delta \Delta^* - v_F^2 p_y^2 \mp V_0) \Phi_2, \end{aligned} \quad (4)$$

with $V_0 = \hbar v_F \sqrt{\Delta_r^2(x) [\partial_x \theta(x)]^2 + [\partial_x \Delta_r(x)]^2}$. Now the DBdG equation is mapped to the Schrödinger equation and the normalization condition is changed to $\int \Psi_1^* \Psi_1 d\mathbf{r} = 1$ and $\int \Phi_2^* \Phi_2 d\mathbf{r} = 1$. The quantization relationships are $\int_{L_E}^{R_E} p_x^\pm dx = (\frac{1}{2} + n)\pi\hbar$ by letting $p_x^\pm = (E^2 - \Delta \Delta^* - v_F^2 p_y^2 \mp V_0)^{1/2}/v_F$. The $\partial_x \theta(x)$ terms in V_0 mean that phase variation provides an alternative method for creating effective potential wells for bound states.

The bound states obtained by the substitutions in Eq. (3) are exact for real gap functions Δ or Δ with a constant phase θ and approximate for slowly varying $\theta(x)$. The π junction and 0 junction studied in this paper belong to the former type; in S2A in [24] we give an example of the latter type. Details about Eq. (3) are in S2A in [24]; in addition, the completeness proof of these bound states still needs further analysis. The coefficients in the substitution between Ψ_1 and Φ_2 must be continuous, and as it is proportional to the argument of $\rho = \partial_x \Delta_r(x) + i \Delta_r(x) \partial_x \theta(x)$, ρ cannot cross the branch point zero. If ρ crosses the branch point, we must multiply a factor $e^{i\pi}$ in the substitution to recover the continuous wave functions and V_0 changes accordingly. One forbidden and two

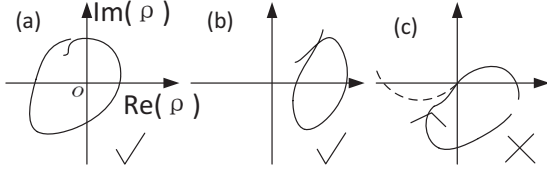


FIG. 2. Depictions of possible trajectories of $\rho(x)$. (a) and (b) do not cross the branch point, while (c) crosses. To avoid the branch point, the dashed line in (c) is the corrected trajectory after a π -phase rotation.

allowed trajectories of $\rho(x)$ are drawn in Fig. 2. The dashed line in Fig. 2(c) shows how to avoid the branch point. The 0 junction discussed later is an example of Fig. 2(c) type.

B. Case of $k_y = 0$ and $E_F \neq 0$

Derived from the DBdG equation with $k_y = 0$, we have the equations

$$\begin{aligned} H_0^2 \Psi + [(H_0 + E_F)\Delta]\Phi &= (E^2 - \Delta\Delta^*)\Psi, \\ H_0^2 \Phi - [(H_0 + E_F)\Delta^*]\Psi &= (E^2 - \Delta\Delta^*)\Phi. \end{aligned} \quad (5)$$

We assume $\Psi(x)[\Phi(x)] = \Psi'(x)[\Phi'(x)]e^{ik_F x}$ with $\hbar v_F k_F = E_F$. The substitutions $\Psi_1 = \Psi_2$ and $\Phi_1 = \Phi_2$ near the Fermi wave vector k_F yield

$$\begin{aligned} -\hbar^2 v_F^2 \partial_x^2 \Psi_1 - i\hbar v_F (\partial_x \Delta)\Phi_2 &= (E^2 - \Delta\Delta^*)\Psi_1, \\ -\hbar^2 v_F^2 \partial_x^2 \Phi_2 + i\hbar v_F (\partial_x \Delta^*)\Psi_1 &= (E^2 - \Delta\Delta^*)\Phi_2, \end{aligned} \quad (6)$$

where the wave functions are in the reduced form $\Psi(\Phi) \rightarrow \Psi(\Phi)e^{-ik_F x}$ to cancel the common $e^{ik_F x}$ terms. Similarly, we can get these equations near $-k_F$ by the substitutions $\Psi_1 = -\Psi_2$ and $\Phi_1 = -\Phi_2$. The formula in the abstract includes two directions $\pm x$ of the momentum. To be concise, we consider the momentum near p_F . If the $\partial_x \Delta$ and $\partial_x \Delta^*$ terms are negligible, we have the relationship $\int_{L_E}^{R_E} (p - p_F) dx = (\frac{1}{2} + n)\pi\hbar$ by letting $p = (E^2 - \Delta\Delta^*)^{1/2}/v_F + p_F$.

To include the $\partial_x \Delta$ and $\partial_x \Delta^*$ terms, using the substitution in Eq. (3), we obtain the same equations in Eq. (4). The quantization relationships are $\int_{L_E}^{R_E} \Delta p^\pm dx = (\frac{1}{2} + n)\pi\hbar$ by letting $\Delta p^\pm = (E^2 - \Delta\Delta^* \mp V_0)^{1/2}/v_F$.

The conditions $\Psi_1 = +(-)\Psi_2$ and $\Phi_1 = +(-)\Phi_2$ can be regarded as the $+x$ - ($-x$ -) moving electron and the $-x$ - ($+x$ -) moving hole (also see the Appendix in Ref. [23]). Whether the assumptions $\Psi_1 = \pm\Psi_2$ and $\Phi_1 = \pm\Phi_2$ are satisfied needs to be checked. In particular, for the π and 0 junctions discussed below, these assumptions are shown to be rigorous in S2B in [24]. According to S2B, we observe that $\int_{L_E}^{R_E} \Delta p^\pm dx = (\frac{1}{2} + n)\pi\hbar$ capture the bound states in both assumptions except for the zero-mode degeneracy.

C. Case of $|\hbar v_F k_y| \ll E_F$

We continue from Eq. (5). Let $k_{Fy} = k_y$, the Fermi wave vector $\mathbf{k}_F = (k_{Fx}, k_{Fy})$, and $\hbar v_F |\mathbf{k}_F| = E_F$. The k_{Fy} is a good

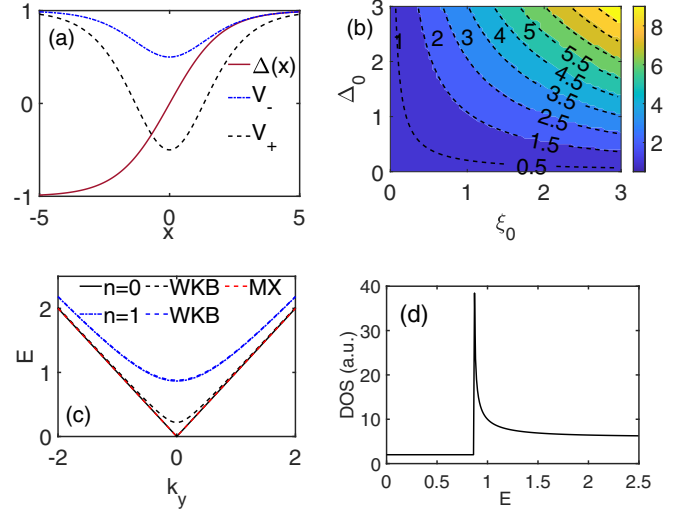


FIG. 3. (a) Example of the π -junction gap function $\Delta(x)$ and the effective potentials V_\pm with $\xi_0 = 2$ and $\Delta_0 = 1$. (b) Phase diagram of the number of bound-state energy levels where the black dashed contour lines are the possible maximum phase accumulation in V_+ for certain ξ_0 and Δ_0 . The integers in the phase regions denote the number of energy levels, and the half integers on the contour lines denote the largest phase integrals with the unit π . (c) Energy spectrum of E versus k_y for the two bound-state levels in V_+ with $\xi_0 = 2$ and $\Delta_0 = 1$. The solid ($n = 0$) and dash-dotted ($n = 1$) lines are the exact results and the dashed lines are the corresponding results the WKB method gives. The exact result for $n = 0$ and the result (MX) by Ma and Xu's quantization condition coincide. The exact result and WKB result for $n = 1$ almost coincide. Note that $n = 1$ in V_+ corresponds to $n = 0$ in V_- , which is not plotted. (d) The DOS plot of the energy spectrum in (c). For all plots, $E_F = 0$.

quantum number. We express Ψ and Φ as

$$\begin{pmatrix} 1e^{i\mathbf{k}_F \mathbf{r}} \cdot a(x) \\ \frac{k_{Fx} + ik_{Fy}}{\sqrt{k_{Fx}^2 + k_{Fy}^2}} e^{i\mathbf{k}_F \mathbf{r}} \cdot b(x) \end{pmatrix} \quad (7)$$

and define $\Psi^x = (a(x), b(x))^T$ and $\Phi^x = (a'(x), b'(x))^T$. Since $|\hbar v_F k_y| \ll E_F$, we can make the approximations $a(x) \approx b(x)$ and $a'(x) \approx b'(x)$. Then we have

$$\begin{aligned} H_0^2 \Psi^x + (H_0 \Delta)\Phi^x &\approx (E^2 - \Delta\Delta^*)\Psi^x, \\ H_0^2 \Phi^x - (H_0 \Delta^*)\Psi^x &\approx (E^2 - \Delta\Delta^*)\Phi^x, \end{aligned} \quad (8)$$

where $H_0 \rightarrow H_0 + E_F$ to cancel E_F . The following procedure is similar to that in the preceding section. Therefore, the quantization relationships are $\int_{L_E}^{R_E} \Delta p^\pm dx = (\frac{1}{2} + n)\pi\hbar$. These discussions are invariant for negative E_F cases except that the positions of the electron and hole bands are exchanged.

D. The π junction and 0 junction

We consider $E_F \approx 0$ and the π -junction gap function $\Delta(x) = \Delta_0 \tanh(x/\xi_0)$, with Δ_0 a constant and ξ_0 a dissipating length concerning the BCS coherence length and the junction width. Therefore, the gap functions on the left- and right-hand sides tend to $\mp\Delta_0$, respectively, as shown in Fig. 3(a), which

means a π -phase shift. We make the following discussion based on the results in Sec. II A.

For the π junction, we should include the $\partial_x \Delta$ and $\partial_x \Delta^*$ terms. With a fixed p_y , using the substitution

$$\Psi_1 = \pm i \Phi_2, \quad (9)$$

we obtain

$$\begin{aligned} v_F^2 \hat{p}_x^2 \Psi_1 + [\Delta \Delta^* \mp \hbar v_F \partial_x \Delta(x)] \Psi_1 &= (E^2 - v_F^2 p_y^2) \Psi_1, \\ v_F^2 \hat{p}_x^2 \Phi_2 + [\Delta \Delta^* \mp \hbar v_F \partial_x \Delta^*(x)] \Phi_2 &= (E^2 - v_F^2 p_y^2) \Phi_2. \end{aligned} \quad (10)$$

The quantization conditions are $\int_{L_E}^{R_E} p_x^\pm dx = (\frac{1}{2} + n)\pi \hbar$ by letting $p_x^\pm = [E^2 - v_F^2 p_y^2 - \Delta \Delta^* \pm \hbar v_F \partial_x \Delta(x)]^{1/2} / v_F$.

We let $\hbar = v_F = 1$. The effective potentials are $V_\pm = \Delta \Delta^* \mp \hbar v_F \partial_x \Delta(x) = \Delta_0^2 \tanh^2(x/\xi_0) \mp \frac{\Delta_0}{\xi_0} \text{sech}^2(x/\xi_0)$, which is the Rosen-Morse potential [26] considering $\tanh^2(x/\xi_0) = 1 - \text{sech}^2(x/\xi_0)$; an example is shown in Fig. 3(a). The exact bound-state energy is given by $E_+(n, k_y) = \sqrt{\Delta_0^2 - (\Delta_0 - \frac{n}{\xi_0})^2 + k_y^2}$ with $\Delta_0 - \frac{n}{\xi_0} \geq 0$ and $E_-(n, k_y) = \sqrt{\Delta_0^2 - (\Delta_0 - \frac{n+1}{\xi_0})^2 + k_y^2}$ with $\Delta_0 - \frac{n+1}{\xi_0} \geq 0$. When using dimensional units, we only make the substitutions $1/\xi_0 \rightarrow \hbar v_F / \xi_0$ and $k_y \rightarrow v_F p_y$. Here E_\pm correspond to the bound states in V_\pm and we note that $E_+(n+1, k_y) = E_-(n, k_y)$. The phase diagram of the number of bound-state energy levels is shown in Fig. 3(b). The dashed lines are the value of $\int_{L_{E_m}}^{R_{E_m}} p_x^+ dx$, where $E_m = \sqrt{k_y^2 + \Delta \Delta^*}$ is the possible maximum bound-state energy. The integral $\int_{L_{E_m}}^{R_{E_m}} p_x^+ dx$ means the possible maximum phase accumulation within V_+ ; hence one more bound-state level appears every time $\int_{L_{E_m}}^{R_{E_m}} p_x^+ dx$ adds π . The energy levels above the 0.5π phase line are well described by the WKB method, while the first bound states with small ξ_0 and Δ_0 are beyond the WKB domain. However, the $n=0$ bound states have analytical solutions, i.e., the Majorana zero modes. The zero modes have twofold degeneracy counting both the time-reversal and particle-hole symmetries $\mathcal{M}_1 = (1, 0, 0, -i)^T \exp[-\int_0^x \Delta(x') dx']$ and $\mathcal{M}_2 = (0, 1, -i, 0)^T \exp[-\int_0^x \Delta(x') dx']$ with $k_y = 0$.

The WKB results are approximate. To realize the exact results, we must use the exact quantization condition [7] or equivalently add a correction term to the WKB quantization condition. The exact quantization condition for $n=0$ in V_+ is $\int_{L_E}^{R_E} p_x^+ dx = (\frac{1}{2} + \nu)\pi$ with the correction index $\nu = \frac{1}{2} + \sqrt{1 + \Delta_0 \xi_0} (\sqrt{\Delta_0 \xi_0} - \sqrt{1 + \Delta_0 \xi_0})$, and ν is invariant to n according to Ma and Xu's conclusions [7]. We obtain $\nu \approx -0.05$ for $\xi_0 = 2$ and $\Delta_0 = 1$. Now the zero modes are recovered as shown in Fig. 3(c) and these correspond to the zero-point energy in the WKB formalism. Note that we can find the correction term even when the exact E_\pm and constructed eigenvectors are unknown, yet an analytical ν may not be available for general inexactly solvable effective potentials.

Now we turn to degeneracy. The first energy level with $k_y \neq 0$ is not degenerate. Starting from the second energy level, (E, k_y) bound states are doubly degenerate originating from the time-reversal symmetry of the motion in the x direction. These properties can be explained by the difference

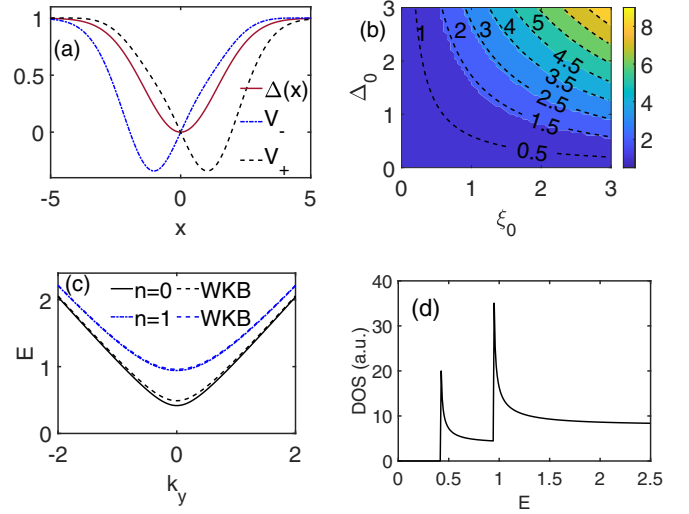


FIG. 4. (a) Example of the 0-junction gap function $\Delta(x)$ and the effective potentials V_\pm for $\xi_0 = 2$ and $\Delta_0 = 1$. (b) Phase diagram of the number of bound-state energy levels; the other information is similar to that in Fig. 3(b). (c) Energy spectrum of E versus k_y for the two bound-state levels at $\xi_0 = 2$ and $\Delta_0 = 1$; the other information is similar to that in Fig. 3(c). (d) The DOS plot of the energy spectrum in (c). For all plots, $E_F = 0$.

between the two effective potentials V_\pm . The first energy level only exists in V_+ , which is lower. In contrast, the two degenerate bound states in higher levels exist in both V_\pm , which gives twofold degeneracy. As mentioned previously, the zero modes are special because of the symmetry and two-component spinors. If we check the wave functions of the two degenerate bound states in V_\pm , the one in V_+ has one more node than the other in V_- because these have different bound state numbers in the WKB formalism. Similar results are also given by the transfer-matrix method despite different boundary conditions [18]. If choosing some other gap functions with smaller variations in the middle area of the junction, we possibly see that the effective potentials have double wells where Andreev bound states may oscillate between two wells, which can be solved by the WKB approximation as well.

As a comparison, we discuss a zero-phase Gaussian-like gap function $\Delta(x) = \Delta_0(1 - \eta e^{-(x/\xi_0)^2})$, with Δ_0 a constant and η and ξ_0 two coefficients concerning the junction width and the BCS coherence length. In this discussion, we take $\eta = 1$, which may describe a critical junction width with which the pairing parameter almost vanishes in the middle. The phase diagram in Fig. 4(b) of the number of bound states levels is similar to the π junction. However, the energy spectrum is fundamentally different. The bound-state excitation spectrum in Fig. 4(c) is gapped, which is also shown in the density of states (DOS) plot in Fig. 4(d) where two Van Hove singularities are caused by the two flat bottoms of the two bands. Since two effective potentials in Fig. 4(a) are symmetric about each other, (E, k_y) states are all doubly degenerate. From another perspective, the twofold degeneracy originates from the time-reversal symmetry of the motion in the x direction.

III. SEMIMETALS WITH PARABOLIC DISPERSION RELATIONSHIPS

Briefly, the BdG equation will be reduced to a fourth-order differential equation; then we analyze the asymptotes, which is followed by the treatment of the turning points. After approximations, the wave functions obtained by the Frobenius method around the turning points approach the asymptotes. The quantization condition is derived through the relationships between these wave functions. The detailed proof is given in S2C in [24].

We use a simple Hamiltonian $H_0 = \frac{\hat{p}_x^2}{2m}\sigma_x - E_F$, with m the effective mass to model the bipartite semimetal with a parabolic dispersion relationship. The bilayer graphene under low-energy approximation may be a typical example despite the minor difference in the Hamiltonian [27,28]. We first assume $p_y(p_z) = 0$ and $E_F = 0$, and physically $p_y(p_z)$ should not affect the quantization condition in the x direction, which will be illustrated later. We consider negligible phase variation and use the simplified notation $\Delta^* \rightarrow \Delta$. The corresponding BdG equation is

$$(H_0\tau_z + \Delta\tau_x)\Lambda = E\Lambda, \quad (11)$$

where $\Lambda = [(\Psi_1, \Psi_2), (\Phi_1, \Phi_2)]^T$ and the τ are Pauli matrices. The excitation spectrum for uniform $\Delta(x)$ is $E = \sqrt{(\mathbf{p}^2/2m)^2 + \Delta^2}$, where the electronlike and holelike bands coincide. The corresponding mean-field Hamiltonian may be written as $\mathcal{H} = \int [\sum_{\sigma} (\Upsilon_{1,\sigma}^\dagger, \Upsilon_{2,\sigma}^\dagger) H_0 (\Upsilon_{1,\sigma}, \Upsilon_{2,\sigma})^T + (\Upsilon_{1,\uparrow}^\dagger, \Upsilon_{2,\uparrow}^\dagger) \Delta I (\Upsilon_{1,\downarrow}, \Upsilon_{2,\downarrow})^T + \text{H.c.}] d\mathbf{r}$, with Υ the field operator and σ the \uparrow and \downarrow spins. After some substitutions, we get

$$\left(\frac{\hbar^2}{2m}\right)^2 \partial_x^4 \Psi_1(\Phi_2) = [E^2 - \Delta(x)^2] \Psi_1(\Phi_2), \quad (12)$$

where we have discarded the derivative terms of Δ as we assume that the gap function changes slowly. As the two equations are equivalent, we study one of them: $(\frac{\hbar^2}{2m})^2 \partial_x^4 \Psi_1 = (E^2 - \Delta^2) \Psi_1$.

In S2C in [24] we use the GWKB method to prove that the quantization condition for Eq. (12) is $\int_{L_E}^{R_E} p dx = (\frac{1}{2} + n)\pi\hbar$, where $p = \hbar k_0$, with $k_0 = (\frac{E^2 - \Delta^2}{\hbar^2/2m})^{1/4}$. Our formulas are also verified by the numerical simulations of the original equations in S1C in [24].

According to the Heisenberg uncertainty principle, the coherence length is $\xi_0 \sim \hbar/\Delta p$ [29], which is at the same magnitude as the electron wavelength $\lambda = \hbar/p$. This is a major approximation, since generally $\xi_0 \gg \lambda$ in BCS superconductors. However, we also note that the flat band may promote the possibility of BCS superconductivity [30–32]. The enhancement of the density of states near the flat band may make the mean-field BCS mechanism effective. As our model for the Schrödinger fermions also has a Van Hove singularity at the Fermi level, it is a potential platform for superconductivity.

The momenta in other directions are good quantum numbers, which physically do not affect this quantization rule for $E_F \approx 0$. Relevant discussions are provided in Sec. V A.

IV. SCHRÖDINGER FERMIONS

The kinetic energy in the y and z directions can be absorbed by E_F for Schrödinger fermions: $\frac{\hat{p}_x^2}{2m} - E_F \rightarrow \frac{\hat{p}_x^2}{2m} - E'_F$. Hence, we only consider the one-dimensional BdG equation

$$E\Lambda = \left[\left(-\frac{\hbar^2 \partial_x^2}{2m} - E_F \right) \sigma_z + \Delta(x) \sigma_x \right] \Lambda, \quad (13)$$

where $\Lambda = (\Psi, \Phi)^T$ and Ψ (Φ) is the one-component electron (hole) wave function. The excitation spectrum for uniform $\Delta(x)$ is $E = \sqrt{(p_x^2/2m - E_F)^2 + \Delta^2}$. We assume $E_F \gg \Delta$ and E and ignore the phase variation of Δ . By canceling Φ and dropping the derivatives of Δ , we have

$$\left(\frac{\hbar^2}{2m}\right)^2 (-\partial_x^2 - k_F^2)^2 \Psi(x) = (E^2 - \Delta^2) \Psi(x). \quad (14)$$

In contrast, Ref. [16] includes the phase change, and the final result therein only depends on the phase difference of the two superconductors in a constriction with slight separation between the two superconductors. As explained in Sec. V A, our formalism may also include the phase change by $\Delta^2 \rightarrow \Delta\Delta^*$ for specific gap functions.

In S2D in [24] we derive the quantization condition of the bound states in Eq. (14) and our treatment includes more details than Andreev's simplifications. Letting $\bar{k} = \frac{(E^2 - \Delta^2)^{1/2}}{v_F \hbar}$, the result is $\int_{L_E}^{R_E} \bar{k} dx = (n + \frac{1}{2})\pi$, i.e., $\int_{L_E}^{R_E} |\mathbf{p} \pm \mathbf{p}_F| dx = (n + \frac{1}{2})\pi\hbar$. In three-dimensional materials, k_y and k_z can be absorbed by E_F and \mathbf{p}_F ; for this reason, we use vectors.

To compare with others' results, when $\Delta = 0$ in the normal layer with the distance d of an SNS junction, the bound states are $E = (n + \frac{1}{2})\pi\hbar v_F/d$ with the degeneracy 4 (spin included). This formula takes an additional $\frac{1}{2}\pi\hbar$ compared with Andreev's bound states and agrees with Kūlik's result when $E \ll \Delta_0$, the superconducting gap, and the phase difference $\chi = 0$.

From the previous discussions of massless Dirac fermions and Schrödinger fermions, we find that the quantization condition for the bound states with $E_F \gg \Delta$ and E mainly depends on the excitation spectrum in the homogeneous limit rather than the original dispersion relationship. The reason is apparent. For $E_F \gg \Delta$ and E , the band distinction disappears between different dispersions near E_F in the scale of E .

V. OTHER APPLICATIONS

In Sec. IID we discussed the π junction and 0 junction for massless Dirac fermions. Here we discuss applications for Schrödinger fermions and semimetals with parabolic dispersion relationships.

A. SNS junctions

We consider the following gap function induced by the proximity effect inside the normal layer $-d/2 < x < d/2$ [33]:

$$\Delta(x) = \Delta_L e^{-(x+d/2)/\xi} + \Delta_R e^{-(d/2-x)/\xi}. \quad (15)$$

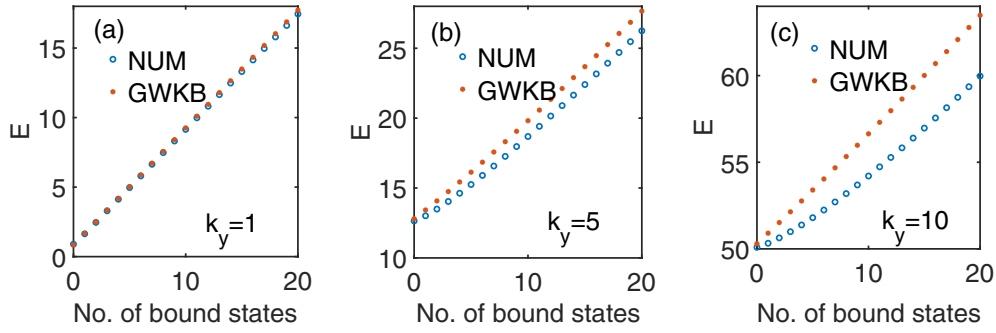


FIG. 5. Numerical results (NUM) and the results by the rough formula based on the GWKB method for the semimetal with $E_F \sim 0$. For small k_y , we see that even the rough formula works well, and we can adjust the function $\overline{\Delta}^2$ to improve the approximation.

Here $\xi \propto \frac{1}{(T-T_c)^{1/2}}$ is the Ginzburg-Landau coherence length and Δ_L and Δ_R are the gap functions with the same magnitude Δ_0 at the left and right sides, respectively. According to the Josephson effect, the Josephson current $J_s \propto \sin \chi$, with χ the phase difference between Δ_L and Δ_R .

Kulik considered the case $d \gg \xi_0$, the BCS coherence length under the extremely-low-temperature condition $T \ll T_c$. In Kulik's bound states, a coherent connection between Δ_L and Δ_R exists through the bound states and this yields that the discrete energy levels depend on the phase difference. Here, to show one application of our theory on the Josephson effect, we consider that $2\xi \lesssim d \lesssim 4\xi$ with T not very close to T_c . Then we make the following approximation to simplify $\Delta\Delta^*$:

$$\begin{aligned} \Delta\Delta^* &= \Delta_0^2 e^{-2(x+d/2)/\xi} + \Delta_0^2 e^{-2(d/2-x)/\xi} + 2\Delta_0^2 e^{-d/\xi} \cos \chi \\ &\approx \Delta_0^2 e^{-d/\xi} \left(\frac{4e^{d/\xi} - 8}{d^2} x^2 + 2 + 2 \cos \chi \right) = \eta_1 x^2 + \eta_2. \end{aligned} \quad (16)$$

According to the conclusion about Schrödinger fermions, when $E_F \gg \Delta$ and E , we have

$$\int_{L_E}^{R_E} \frac{(E^2 - \Delta\Delta^*)^{1/2}}{\hbar v_F} dx = \left(n + \frac{1}{2} \right) \pi. \quad (17)$$

Therefore,

$$E_n = \left[2\sqrt{\eta_1} \hbar v_F \left(n + \frac{1}{2} \right) + \eta_2 \right]^{1/2}. \quad (18)$$

The $\cos \chi$ term in η_2 leads to the Josephson effect because roughly we observe $dE_n/d\chi \propto \sin \chi$ [34].

When $E_F \sim 0$ for the semimetal with a parabolic dispersion relationship, from the previous discussion, the quantization rule is

$$\int_{L_E}^{R_E} \frac{(E^2 - \Delta\Delta^*)^{1/4}}{(\hbar^2/2m)^{1/2}} dx = \left(n + \frac{1}{2} \right) \pi. \quad (19)$$

As a result, the discrete levels are given by

$$E_n = \left[\left(\frac{3\Gamma(\frac{1}{4})(n + \frac{1}{2})\pi^{3/2}\sqrt{\eta_1}(\hbar^2/2m)^{1/2}}{4\Gamma(\frac{3}{4})} \right)^{4/3} + \eta_2 \right]^{1/2}. \quad (20)$$

In the case of a semimetal with $E_F \sim 0$, as other momentum components are good quantum numbers, according to the

excitation spectrum with uniform $\Delta(x)$, $E = \sqrt{(\mathbf{p}^2/2m)^2 + \Delta^2}$, the quantization rule may be modified by $\int_{L_E}^{R_E} p_x dx = \left(\frac{1}{2} + n \right) \pi \hbar$, with $p_x = \sqrt{2m\{[E(n, k_y, k_z)^2 - \Delta\Delta^*]^{1/2} - E_q\}}$ and $E_q = \frac{\hbar^2 k_y^2}{2m} + \frac{\hbar^2 k_z^2}{2m}$. This integration is generally difficult; to obtain a rough analytical expression we approximate the bound-state energy by $E(n, k_y, k_z)^2 = E_0(n)^2 + E_q^2 + 2E_q\sqrt{E_0^2 - \overline{\Delta}^2}$, where $E_0(n)$ is the bound-state energy for $(k_y, k_z) = \mathbf{0}$ and $\overline{\Delta}^2$ is an adjustable function based on the form of the gap function. The term $\sqrt{E_0^2 - \overline{\Delta}^2}$ can be considered as a dressed kinetic energy in the x direction and the coupling term $E_q\sqrt{E_0^2 - \overline{\Delta}^2}$ between different directions is analogous to the coupling term within $(\mathbf{p}^2/2m)^2$. In Fig. 5 we compare the numerical values and the approximate values by choosing $\Delta = \frac{1}{2}x^2$ and $\overline{\Delta}^2 = E_0^2/2$ for a two-dimensional semimetal. As shown, the small difference for small k_y verifies the effectiveness of this simplified bound-state energy. Such a rough analytical expression for the bound-state energy should already be helpful for many problems, and we can optimize $\overline{\Delta}^2$ to obtain more precise results. An alternative method is determining the integral numerically, which is more precise and still convenient.

B. Excitation threshold

de Gennes used the variation method to calculate the excitation threshold in nonuniform superconductors in Chap. 5 of Ref. [35]. In this section we compare our result with his.

de Gennes considered a parabolic order parameter with the minimum Δ_{\min} ,

$$\Delta(x) = \Delta_{\min} \left(1 + \frac{x^2}{\delta^2} \right), \quad (21)$$

and obtained the threshold energy

$$E_0^2 = \Delta_{\min}^2 (1 + \mu^{2/3}), \quad (22)$$

where $\mu \sim \frac{\hbar^2}{2m\delta^2\Delta_{\min}}$. In addition, de Gennes gave an estimate example: Given $\delta \sim \frac{\hbar v_F}{\Delta_{\min}}$, $\mu \sim 10^{-2}$.

Substitution of $n=0$ in our quantization rule for Schrödinger fermions with large E_F gives the threshold

energy

$$E_0^2 = \Delta_{\min}^2 \left(1 + \frac{\sqrt{2}\hbar v_F}{\delta \Delta_{\min}} \right). \quad (23)$$

Given the same δ , we have $E_0^2 = \Delta_{\min}^2 (1 + \sqrt{2})$, showing a significant error compared with de Gennes's result. This is a reasonable error because the basis of the WKB and our approximation is slowly changing $\Delta(x)$ and small derivative terms of $\Delta(x)$ in Eq. (14). Apparently, this δ value is not in our range when Δ_{\min} is not small. If we adjust $\delta \gg \frac{\hbar v_F}{\Delta_{\min}}$, the conclusions of the two results are consistent, i.e., $E_0 \simeq \Delta_{\min}$.

Alternatively, a faster approach is to use the limit $v_F \sim 0$ to achieve the same result. There are three reasons. The first is because de Gennes actually uses k_{\perp} in a direction perpendicular to the x direction to cancel the Fermi energy, which results in an effective $E_F \sim 0$ in the x direction; the second is that v_F in our formalism is the velocity in the x direction since our problem is reduced to a one-dimensional problem; and the third is that we can get the $v_F \sim 0$ limit for the reduced $E_F \sim 0$ based on our empirical formula. Therefore, the method taken by de Gennes in fact leads to our formalism.

C. Tunneling

Andreev reflection tells us that a hole will be reflected when an electron in a normal metal flows into a superconductor. Therefore, two electrons are absorbed by the superconductor to form one Cooper pair. However, if the superconductor layer has a finite width, there is a possibility for the unpaired electrons to escape the superconductor. Now we calculate the tunneling probability in an NSN junction with a finite but large width $L \gg \xi_0$ of the superconductor layer. Since the width of the superconductor is large, the crossed Andreev reflection can be ignored.

We discuss Schrödinger fermions with $E_F \gg \Delta$ and E , and $\Delta = 0$ in the normal layers. The incident electron has the wave function

$$\psi_i = e^{ik_1 x} \begin{pmatrix} 1 \\ 0 \end{pmatrix}, \quad (24)$$

with $k_1 = k_F + \frac{E}{v_F \hbar}$. The reflected wave is

$$\psi_r = r_h e^{ik_2 x} \begin{pmatrix} 0 \\ 1 \end{pmatrix} + r_e e^{ik_3 x} \begin{pmatrix} 1 \\ 0 \end{pmatrix}, \quad (25)$$

with $k_2 = k_F - \frac{E}{v_F \hbar}$, $k_3 = -k_1$, and r_h (r_e) the reflected amplitude for the hole (electron). In the superconductor region $0 < x < L$, our approximation gives

$$\psi_s(x) = \frac{C}{\sqrt{\kappa(x)}} \exp\left(\int_0^x \kappa_1 dx'\right) \begin{pmatrix} 1 \\ \gamma \end{pmatrix}, \quad (26)$$

with $\kappa_1 = ik_F - \frac{(\Delta^2 - E^2)^{1/2}}{\hbar v_F}$, C a constant, γ a ratio, and $\kappa(x) = \frac{(\Delta^2 - E^2)^{1/2}}{\hbar v_F}$. The tunneling probability is given by

$$\begin{aligned} \tilde{T} &\sim \frac{|\exp(-\int_0^L \kappa dx')|^2}{1^2} \\ &= \exp\left(-2 \int_0^L \kappa dx'\right). \end{aligned} \quad (27)$$

VI. DISCUSSION

These bound states manifest themselves in low-temperature and -energy experiments. For example, Andreev discussed the thermodynamics of these bound states, which is important for very low temperatures, typically approximately 0.1 K for $v_F \sim 10^6$ m/s and the normal layer thickness of approximately $10^2 \mu\text{m}$ [20]. Titov *et al.* studied the thermal conductance of Andreev modes which is realized by the specular Andreev reflection in a graphene channel with superconducting boundaries [18]. These bound states are also characterized by infrared spectroscopy if we shed low-frequency light on superconductors. The photon energy should be controlled to be comparable to the bound-state energy difference and smaller than the excitation energy of Cooper pairs. These features may be exploited to examine whether a superconductor has defects in specific regions and the size of the defects.

For the experimental realization, as mentioned by de Gennes, the spatial variation of $\Delta(x)$ can be fabricated by depositing different metals on thin superconductors [35]. The order parameter depends on many variables, leading to other possible methods. For instance, we can continuously dope or change the materials of a bulk superconductor in one direction to adjust the order parameter; for thin samples, the temperature gradient also yields varying $\Delta(x)$, etc.

Regarding moderate E_F , it is not rigorously determined whether Schrödinger fermions still have such a concise quantization rule, while the large E_F condition is not necessary for Dirac fermions with $k_y = 0$ presenting the advantage of generality. Momenta in other directions also cause difficulty. However, in particular, when extreme precision is not required, our experience and viewpoint are that the GWKB (WKB included) and Bohr-Sommerfeld quantization conditions should both work well for broader parameter ranges of nonuniform superconductors. In addition, the GWKB quantization condition should work better if there is no abrupt change in the gap function. The crucial step is finding the proper semiclassical momentum, effective potentials, and \mathbf{p}_F based on the excitation spectrum of homogeneous superconductors (an example is in S1E [24]), since generally we need to deal with the chemical potentials and other momenta or other terms which may couple with the momentum we must know. Special care is required when the excitation spectra have gaps. For example, purely electronlike bound states may exist in the gap between the holelike and electronlike bands [18,23] (also see S1E in [24]).

VII. SUMMARY

We have provided the quantization conditions for the Andreev bound states in the wells of nonuniform superconductors. We have rigorously studied several parameter limits for massless Dirac fermions, semimetals with parabolic dispersion relationships, and Schrödinger fermions. These quantization conditions should be easily applied to many problems concerning Andreev bound states in TI surface states, graphene, and other Dirac materials; semimetals like bilayer graphene; and normal metal superconductors. We also

have provided empirical quantization conditions for other parameter regions as mentioned previously.

We have discussed the π and 0 junctions for the TI surface states as examples and demonstrated the bound-state spectrum and the phase diagram of the number of bound-state levels. The Majorana zero modes in the π junction are found to correspond to the zero-point energy in our method. The Majorana bound state in a vortex may also be understood better in this way. For a vortex $\Delta_0(r)e^{i\vartheta}$ with r and ϑ the polar coordinates, we can do a radial section along a diameter in the vortex and then this section becomes a π junction. Therefore, the Majorana bound state in a vortex should also correspond to the zero-point energy. A detailed analysis is beyond the scope of the present work. In quantum field theory, the zero-point energy is the result of quantum fluctuation of the universe, which has great significance such as the Casimir effect. In analogy to our observation, we may ask whether the

Majorana fermion in high-energy physics comes from vacuum fluctuations.

We have also discussed other applications such as the SNS junctions, excitation threshold, and NSN junctions. In addition, our treatment of a fourth-order differential equation is attributable to progress in mathematical physics. The GWKB method may inspire solutions to other fourth-order or even higher-order Bessel-type ordinary differential equations. In another paper, we exploit the GWKB method to reveal bound states in general higher-order differential equations [36]. The results therein are useful to solve other energy-momentum dispersion relationships such as the cubic dispersion or beyond.

ACKNOWLEDGMENTS

We thank Y. S. An for discussions. This work was supported by the Hong Kong Research Grants Council (Projects No. GRF16300918 and No. 16309020).

-
- [1] S. Weinberg, *Lectures on Quantum Mechanics* (Cambridge University Press, Cambridge, 2015).
- [2] D. J. Griffiths and D. F. Schroeter, *Introduction to Quantum Mechanics* (Cambridge University Press, Cambridge, 2018).
- [3] G. Wentzel, Eine verallgemeinerung der quantenbedingungen für die zwecke der wellenmechanik, *Z. Phys.* **38**, 518 (1926).
- [4] H. A. Kramers, Wellenmechanik und halbzahlige quantisierung, *Z. Phys.* **39**, 828 (1926).
- [5] L. Brillouin, La mécanique ondulatoire de Schrödinger; une méthode générale de résolution par approximations successives, *C. R. Acad. Sci.* **183**, 24 (1926).
- [6] H. Jeffreys, On certain approximate solutions of lineae differential equations of the second order, *Proc. Lond. Math. Soc.* **s2-23**, 428 (1925).
- [7] Z.-Q. Ma and B.-W. Xu, Quantum correction in exact quantization rules, *Europhys. Lett.* **69**, 685 (2005).
- [8] A. Comtet, A. Bandrauk, and D. K. Campbell, Exactness of semiclassical bound state energies for supersymmetric quantum mechanics, *Phys. Lett. B* **150**, 159 (1985).
- [9] A. Khare, How good is the supersymmetry-inspired WKB quantization condition? *Phys. Lett. B* **161**, 131 (1985).
- [10] R. Dutt, A. Khare, and U. P. Sukhatme, Supersymmetry-inspired WKB approximation in quantum mechanics, *Am. J. Phys.* **59**, 723 (1991).
- [11] F. Cooper, A. Khare, and U. Sukhatme, Supersymmetry and quantum mechanics, *Phys. Rep.* **251**, 267 (1995).
- [12] T. Banks, *TCP*, quantum gravity, the cosmological constant and all that..., *Nucl. Phys. B* **249**, 332 (1985).
- [13] T. Singh and T. Padmanabhan, Notes on semiclassical gravity, *Ann. Phys. (NY)* **196**, 296 (1989).
- [14] C. Caroli, P. G. De Gennes, and J. Matricon, Bound fermion states on a vortex line in a type II superconductor, *Phys. Lett.* **9**, 307 (1964).
- [15] J. Bardeen, R. Kümmel, A. Jacobs, and L. Tewordt, Structure of vortex lines in pure superconductors, *Phys. Rev.* **187**, 556 (1969).
- [16] C. W. J. Beenakker and H. van Houten, Josephson Current through a Superconducting Quantum Point Contact Shorter than the Coherence Length, *Phys. Rev. Lett.* **66**, 3056 (1991).
- [17] C. M. Bender and S. A. Orszag, *Advanced Mathematical Methods for Scientists and Engineers I: Asymptotic Methods and Perturbation Theory* (Springer Science + Business Media, New York, 1999), Vol. 1.
- [18] M. Titov, A. Ossipov, and C. W. J. Beenakker, Excitation gap of a graphene channel with superconducting boundaries, *Phys. Rev. B* **75**, 045417 (2007).
- [19] M. Titov and C. W. J. Beenakker, Josephson effect in ballistic graphene, *Phys. Rev. B* **74**, 041401 (2006).
- [20] A. F. Andreev, The thermal conductivity of the intermediate state in superconductors, *Sov. Phys. JETP* **19**, 1228 (1964).
- [21] A. F. Andreev, Electron spectrum of the intermediate state of superconductors, *Sov. Phys. JETP* **22**, 455 (1966).
- [22] I. O. Kulik, Macroscopic quantization and the proximity effect in SNS junctions, *Sov. Phys. JETP* **30**, 944 (1970).
- [23] C. W. J. Beenakker, Specular Andreev Reflection in Graphene, *Phys. Rev. Lett.* **97**, 067007 (2006).
- [24] See Supplemental Material at <http://link.aps.org/supplemental/10.1103/PhysRevB.107.134506> for numerical simulations and detailed proofs of the results in the text. This includes a reference to G. N. Watson, *A Treatise on the Theory of Bessel Functions* (Cambridge University Press, Cambridge, 1995).
- [25] L. Fu and C. L. Kane, Superconducting Proximity Effect and Majorana Fermions at the Surface of a Topological Insulator, *Phys. Rev. Lett.* **100**, 096407 (2008).
- [26] N. Rosen and P. M. Morse, On the vibrations of polyatomic molecules, *Phys. Rev.* **42**, 210 (1932).
- [27] E. McCann and V. I. Fal'ko, Landau-Level Degeneracy and Quantum Hall Effect in a Graphite Bilayer, *Phys. Rev. Lett.* **96**, 086805 (2006).
- [28] T. Ludwig, Andreev reflection in bilayer graphene, *Phys. Rev. B* **75**, 195322 (2007).
- [29] M. Tinkham, *Introduction to Superconductivity* (Courier, Chelmsford, 2004).
- [30] R. Bistritzer and A. H. MacDonald, Moiré bands in twisted double-layer graphene, *Proc. Natl. Acad. Sci. USA* **108**, 12233 (2011).

- [31] Y. Cao, V. Fatemi, S. Fang, K. Watanabe, T. Taniguchi, E. Kaxiras, and P. Jarillo-Herrero, Unconventional superconductivity in magic-angle graphene superlattices, *Nature (London)* **556**, 43 (2018).
- [32] B. Lian, Z. Wang, and B. A. Bernevig, Twisted Bilayer Graphene: A Phonon-Driven Superconductor, *Phys. Rev. Lett.* **122**, 257002 (2019).
- [33] L. Aslamazov, A. Larkin, Y. N. Ovchinnikov, and Z. Fiz, Josephson effect in superconductors separated by a normal metal, *Sov. Phys. JETP* **28**, 171 (1969).
- [34] C. W. J. Beenakker, *Colloquium: Andreev reflection and Klein tunneling in graphene*, *Rev. Mod. Phys.* **80**, 1337 (2008).
- [35] P.-G. de Gennes and P. A. Pincus, *Superconductivity of Metals and Alloys* (CRC, Boca Raton, 2018).
- [36] X. Fan, Quantization condition of the bound states in $e^{-i\pi n/2} \nabla_x^n \Psi = (E - \Delta(x))\Psi$ (unpublished).